

Combined extinction and absorption UV–vis spectroscopy reveals shape imperfections of metallic nanoparticles

Johan Grand, Baptiste Auguié, and Eric C. Le Ru*

The MacDiarmid Institute for Advanced Materials and Nanotechnology, School of Chemical and Physical Sciences, Victoria University of Wellington, PO Box 600, Wellington 6140, New Zealand

E-mail: eric.leru@vuw.ac.nz

Abstract

Metallic nanoparticle solutions are routinely characterized by measuring their extinction spectrum (with UV–vis spectroscopy). Theoretical predictions such as Mie theory for spheres can then be used to infer important properties, such as particle size and concentration. Here we highlight the benefits of measuring not only the extinction (the sum of absorption and scattering) but also the absorption spectrum (which excludes scattering) for routine characterization of metallic nanoparticles. We use an integrating sphere-based method to measure the combined extinction–absorption spectra of silver nanospheres and nanocubes. Using a suite of electromagnetic modeling tools (Mie theory, T-matrix, Surface Integral Equation methods), we show that the absorption spectrum, in contrast to extinction, is particularly sensitive to shape imperfections such as roughness, faceting, or edge rounding. We study in detail the canonical case of silver nanospheres, where small discrepancies between experimental and calculated extinction spectra are still common and often overlooked. We show

1
2
3 that this mismatch between theory and experiment becomes much more important
4 when considering the absorption spectrum, and can no longer be dismissed as exper-
5 imental imperfections. We focus in particular on the quadrupolar localized plasmon
6 resonance of silver nanospheres, which is predicted to be very prominent in the ab-
7 sorption spectrum but is not observed in our experiments. We consider and discuss
8 a number of possible explanations to account for this discrepancy, including: changes
9 in the dielectric function of Ag, size polydispersity, and shape imperfections such as
10 elongation, faceting, and roughness. We are able to pinpoint faceting and roughness
11 as the likely causes for the observed discrepancy. A similar analysis is carried out
12 on silver nanocubes to demonstrate the generality of this conclusion. We conclude
13 that the absorption spectrum is in general much more sensitive to the fine details of a
14 nanoparticle geometry, compared to the extinction spectrum. The ratio of extinction
15 to absorption also provides a sensitive indicator of size for many types of nanopar-
16 ticles, much more reliably than any observed plasmon resonance shifts. Overall, this
17 work demonstrates that combined absorption–extinction measurements provide a much
18 richer characterization tool for metallic nanoparticles.
19
20
21
22
23
24
25
26
27
28
29
30
31
32
33

34 The study of the optical properties of metallic nanoparticles (NPs) began as an attempt
35 to understand fundamental interactions between light and nanomaterials. It has now become
36 a fruitful source of practical applications for physicists, biologists, chemists and engineers,
37 in fields as diverse as drug delivery,¹ nanocatalysis,² single-molecule detection,³ and solar
38 cells.⁴ Following chemical or physical synthesis, NPs are usually thoroughly characterized
39 to verify whether they will serve their intended purpose. UV–vis extinction spectroscopy is
40 the most commonly used tool to measure their optical properties, not only because UV–vis
41 spectrometers are readily available in most labs, but also because it potentially provides
42 indirect information such as size, size distribution, state of aggregation, and NP concen-
43 tration.⁵ For this, the spectra must be compared to theoretical predictions. The optical
44 properties of spheres and spherical nanoshells can be modeled accurately using Mie the-
45 ory,^{6,7} which solves analytically the electromagnetic scattering problem. For more general
46
47
48
49
50
51
52
53
54
55
56
57
58
59
60

1
2
3 nanoparticle shapes, numerical methods such as the finite-difference time domain (FDTD)
4 method,⁸ finite-element method (FEM),⁹ or discrete dipole approximation (DDA)^{10,11} can
5 be used. Accuracy may be difficult to establish with these methods as the finesse of the mesh
6 and/or the size of the bounding box may result in errors.^{12–14} More advanced approaches
7 such as the *T*-matrix^{15–17} or the surface-integral equation (SIE)^{18,19} methods provide more
8 accurate and efficient predictions but are more complicated to implement. It is also worth
9 noting that accurate and simpler approximations exist for NPs that are small enough (typi-
10 cally under 100 nm) in the case of nanospheres and nanoshells,²⁰ nanospheroids,²¹ and even
11 more complex shapes.²² To date, the vast majority of experimental UV–vis spectra have
12 been explained or reproduced using theoretical or numerical predictions, even for relatively
13 complex shapes.^{23–29} Any discrepancy is usually attributed to size distribution (for ensemble
14 measurements),⁵ minor changes in the geometric parameters (which are not always known
15 accurately),^{30,31} or uncertainties in the metal dielectric function.³² With such practical lim-
16 itations in characterizing precisely the samples, the overall fair agreement between theory
17 and experiment suggests that the extinction spectrum does not in fact strongly constrain
18 the nanoparticle properties. We will demonstrate below that absorption spectroscopy can
19 provide much tighter constraints on the precise shape of metal nanoparticles.

20
21
22
23
24
25
26
27
28
29
30
31
32
33
34
35
36
37
38
39
40
41
42
43
44
45
46
47
48
49
50
51
52
53
54
55
56
57
58
59
60

Standard UV–vis spectroscopy measures transmission over a fixed path length (typically 1 cm), from which the extinction spectrum can be inferred (Beer’s law). Although sometimes called an absorption spectrum, it is in fact extinction that is measured – the sum of absorption and scattering of light by the NPs. These two processes are fundamentally different and thus provide different insights into the NPs’ interaction with light. Depending on the application, one may want to exploit one property over the other – for example absorption for photothermal therapy,³³ and extinction for plasmonic sensors.³⁴ Absorption dominates for small NPs, and scattering for large NPs, but for intermediate sizes (in the range 40–100 nm), absorption and scattering can be of a similar order of magnitude.⁷ Some relevant information on the NPs may then be missed by measuring only the extinction spectrum. However,

1
2
3 because of the relative difficulty in measuring absorption spectra, little effort has been dedi-
4 cated to exploiting both extinction and absorption spectra for nanoparticle characterization.
5 Over 30 years ago, Kreibig *et al.*³⁵ used photothermal spectroscopy to show that the two
6 spectra were indeed different. More recently, such measurements have been further improved
7 to measure the absorption spectrum of a single nanoparticle.³⁶⁻³⁸ This approach is however
8 not practical for nanoparticle routine characterization. A simpler method based on measur-
9 ing scattering at 90° has also been proposed^{39,40} but inferring the absorption from it remains
10 very approximate. A more appealing alternative, similar to standard UV-vis in many re-
11 spects, is to place the sample solution inside an integrating sphere and deduce its absorption
12 from a measurement of the sphere throughput.⁴¹ This method has been primarily used in
13 the context of seawater measurements,⁴²⁻⁴⁴ with only sporadic reports of its application to
14 NPs.^{45,46} With careful calibration,^{47,48} the absolute scattering-independent absorption spec-
15 trum can be retrieved, and the scattering spectrum can then be obtained by subtraction
16 from the extinction spectrum. This was measured in Ref.⁴⁵ for silver nanospheres over a
17 wide range of sizes between 30 to 140 nm, but only an approximate calibration was applied
18 to obtain absolute absorption spectra and no comparison was attempted with theory.
19
20
21
22
23
24
25
26
27
28
29
30
31
32
33
34

35 Here we show that an integrating sphere-based measurement of both absorption and ex-
36 tinction UV-vis spectra provides much more insight into the NP properties than the standard
37 extinction-only measurement. We focus in particular on a well-tested system that is used in
38 many applications: 60 nm citrate-coated silver nanospheres dispersed in water. Similar NPs
39 have been used in a number of contexts including surface-enhanced Raman spectroscopy,⁴⁹
40 single-molecule detection,⁵⁰⁻⁵² surface-enhanced fluorescence,⁵³ and molecule-plasmon reso-
41 nance coupling.⁴⁶ We show that while the experimental extinction matches to some extent
42 the theoretical predictions, the absorption spectrum does not, neither in absolute intensity
43 nor in spectral shape. To further investigate these large discrepancies, we use a suite of ac-
44 curate electromagnetic calculation tools, including the Mie theory,⁷ the *T*-matrix method,¹⁶
45 and the surface-integral equation method.¹⁸ By comparing these predictions to our experi-
46
47
48
49
50
51
52
53
54
55
56
57
58
59
60

1
2
3
4
5
6
7
8
9
10
11
12
13
14
15
16
17
18
19
20
21
22
23
24
25
26
27
28
29
30
31
32
33
34
35
36
37
38
39
40
41
42
43
44
45
46
47
48
49
50
51
52
53
54
55
56
57
58
59
60

ments, we discuss possible explanations including: the choice of Ag dielectric function, the elongation of the NP, faceting, and surface roughness. We conclude that these factors typically have a much more pronounced effect on the absorption spectrum than on extinction, emphasizing the importance of the former for routine NP characterization. We also show that the ratio of extinction to absorption provides a strong constraint on the nanoparticle size. Finally, examples of combined absorption/extinction measurements for non-spherical particles, namely silver nanocubes, are also given to further assert the generality of these conclusions. The extension of this approach to gold nanoparticles is also discussed.

Experimental results

Comparisons between experimental and predicted absorption, extinction, and scattering spectra are shown in Fig. 1 in the case of 60 nm-radius Ag nanospheres dispersed in water. In the case of extinction, the agreement between theory and experiment is reasonable but far from perfect. The position of the main dipolar localized surface plasmon (LSP) resonance is predicted at 423 nm and observed at 433 nm. Theory predicts a small peak associated with the quadrupolar LSP at 377 nm, which is not visible in the experiment. The experimental spectrum is also broader than the theoretical one. The latter can however be partly explained by taking into account the unavoidable NP size distribution. This is also shown in Fig. 1 for the size distribution based on TEM analysis (provided by the NP manufacturer), which explains to some extent the broadening. The remaining discrepancy may be attributed to a number of factors including shape distribution, dielectric function, etc, but lacks distinct spectral features to allow for further investigations.

The situation is quite different for the absorption spectrum, where predictions and observations differ significantly in at least two key aspects. Firstly, theory predicts a prominent peak at 377 nm corresponding to the quadrupolar plasmon resonance of the sphere. This remains even for large size distribution (even much larger than shown in the figure) but is not

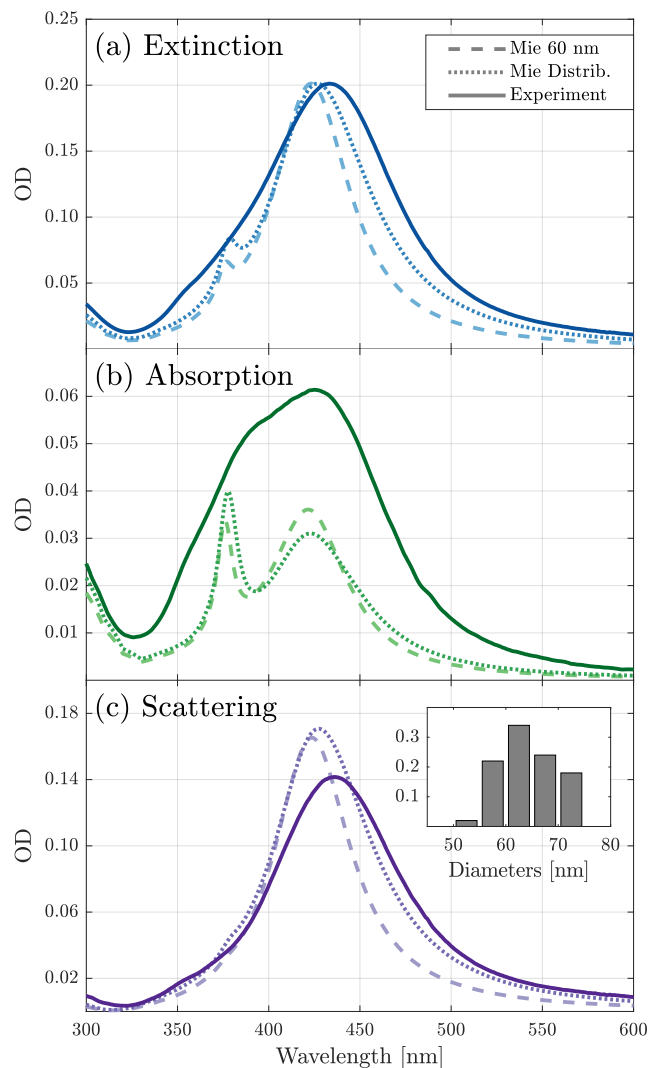


Figure 1: Extinction, absorption, and scattering spectra of a 60 nm spherical silver NP colloidal solution dispersed in water. The experimental data (solid line) is compared to the results of the Mie calculations of a single NP (dashed line) or of a collection of NPs whose size distribution matches that specified by the manufacturer (shown in the inset). In the latter case, the spectra are calculated for each size and weighted by the corresponding probabilities measured from TEM.

observed experimentally. Secondly, the absolute absorbance is much larger than predicted, by as much as a factor of 2 in parts of the spectrum. The NP concentration is here fixed to match the intensity of the extinction spectrum and cannot therefore be adjusted to correct this problem. As a result, the observed scattering spectrum is less intense than predicted. The spectral shape is however similar to predictions, as the quadrupolar resonance is barely

1
2
3 visible in scattering.
4

5 In contrast to extinction, these discrepancies in absorption are now too large to be ig-
6 nored. Understanding their origin might not only improve theoretical predictions of NP
7 optical properties but also help obtain rapid feedback for NP synthesis. In the rest of this
8 paper, we will review and discuss the most likely causes of these discrepancies focusing
9 first on the case of the indiscernible quadrupole resonance in the experimental absorption
10 spectrum.
11
12
13
14
15
16
17
18

19 **Comparison to theoretical results**

20 **Choice of Ag dielectric function**

21
22
23 A key input parameter for any EM simulation involving metallic NPs, is the choice of the
24 dielectric function of the metal. Johnson and Christy's 1972 ellipsometric measurements⁵⁸ of
25 the dielectric function of silver, or analytical fits based on them^{8,56,59} are often used. However,
26 several updated measurements of the dielectric function of the most commonly used metals
27 in plasmonics have recently appeared in the literature.^{32,54,55,57,60,61} These show that Johnson
28 and Christy's data are often inadequate to describe nanoparticles, in particular for silver.
29 Defining a unique dielectric function for metals is indeed difficult, as it can depend on how
30 a particular sample is fabricated. For example, roughness and crystallinity are factors that
31 can greatly influence the optical response of a metal, and therefore its dielectric function.⁵⁷
32 Using the Mie theory, we plot in Fig. 2 the predicted extinction and absorption properties
33 of a 60 nm Ag sphere in water (with dielectric function taken from Ref.⁶²) with different sets
34 of dielectric functions. The main dipolar LSP resonance can be shifted by more than 20 nm,
35 illustrating the critical importance of the choice of the dielectric function. However, the
36 intensity of the quadrupolar mode is relatively unaffected and remains prominent in all cases
37 in the absorption spectrum. This uncertainty cannot therefore explain why the quadrupolar
38 resonance is not observed experimentally. We also note that the choice of dielectric function
39
40
41
42
43
44
45
46
47
48
49
50
51
52
53
54
55
56
57
58
59
60

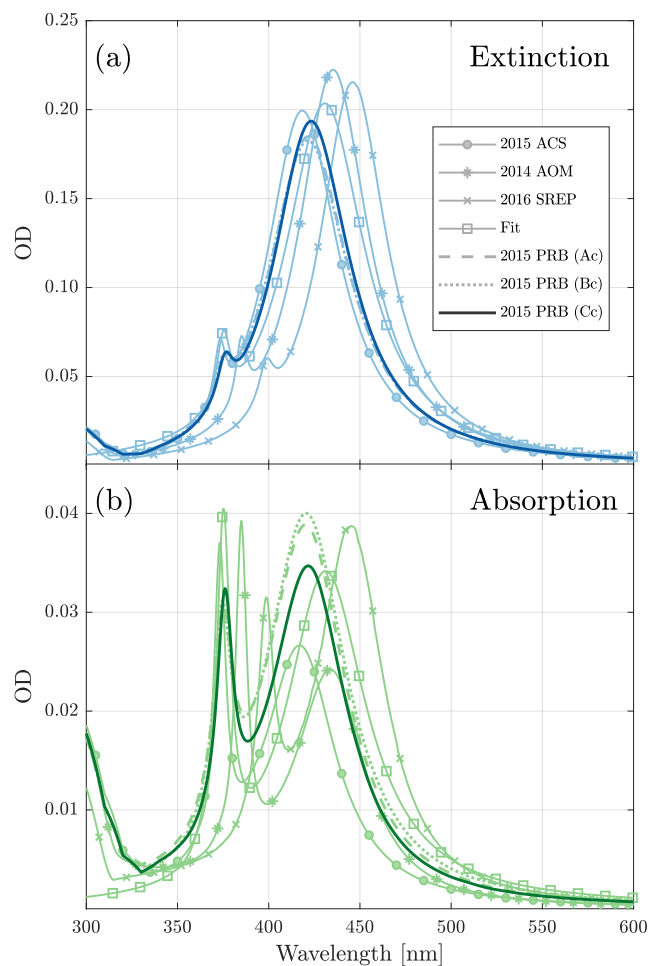


Figure 2: Single-particle extinction and absorption spectra for a 60 nm silver sphere in water, calculated using Mie theory with different sets of dielectric functions: 2015 ACS,⁵⁴ 2014 AOM,⁵⁵ 2016 SREP,³² Fit,⁵⁶ 2015 PRB.⁵⁷ The latter provides 3 different sets of measurements and uses post-processing to ensure Kramers-Krönig consistency (labeled Ac,Bc,Cc). The fit is based on a Drude model fit of the 1972 Johnson and Christy measurement.⁵⁸ The dielectric function used for all other calculations in this article is displayed as the solid line (2015 PRB (Cc)).

may affect the absolute intensity of absorption. It would nevertheless not be sufficient to bridge the intensity gap between the experimental and the predicted absorption. For all the other calculations throughout the article, we chose to use the dielectric function measured and recommended by Yang et al. in Ref.⁵⁷ (`AgC_corrected.csv`, as provided in the supporting information of⁵⁷).

Particle elongation

So far we have considered the NPs as perfect spheres, which greatly simplified the EM simulations, as Mie theory provides an analytical solution to the light scattering problem. The assumption of an idealised spherical shape is however unrealistic. The simplest departure from a spherical shape is its elongation along one axis, which we investigate by considering spheroidal NPs (prolate and oblate). To model their optical response we turn to the *T*-Matrix method,^{15,16} an accurate, fast, and numerically stable¹⁷ solution of the Maxwell equations, from which orientation-averaged properties can be derived with no added computational cost. As we can see in Fig. 3, the dipolar resonance broadens and splits with the dominant peak slightly red-shifted for oblate NPs and blue-shifted for prolate NPs when the aspect ratio is increased, as is well-documented. The spectral position and relative intensity of the quadrupolar mode remains however largely unaffected by the change in aspect ratio. Broadening and splitting of the quadrupolar peak is only predicted to occur for aspect ratios of 1.2 and above, which is much larger than we reasonably expect in our samples. Thus, even considering a distribution of prolate and oblate NPs with different aspect ratio would fail to explain the experimental absorption spectrum.

Faceting

The shape of a NP is greatly affected by its crystalline structure, which governs the growth mechanisms and generates faceted particles; imperfections in growth can lead to particles with different number or types of facets.⁶³ Although evident in TEM images of nanospheres, especially for silver (see for example inset in Fig. 4), facets are usually ignored in theoretical predictions for spherical NPs because of the added complexity. To predict the optical properties of faceted NPs we use the Surface Integral Equation (SIE) method, which has been shown to be particularly accurate for plasmonic NPs of arbitrary shapes.^{18,19,64} SIE allows modeling of any kind of particle shape by meshing its surface. It presents many advantages over other commonly-used numerical methods discretizing the entire volume of

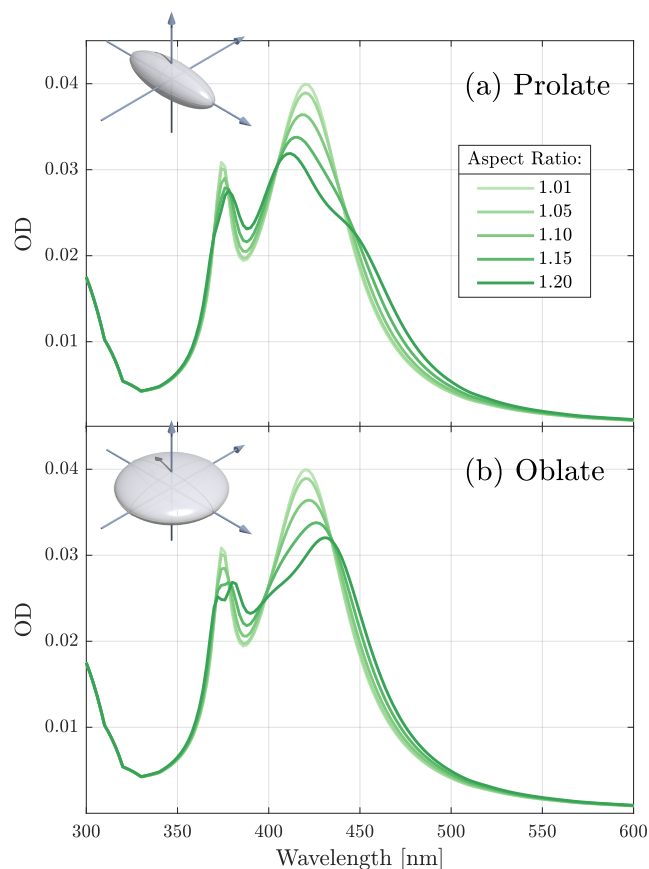


Figure 3: Absorption spectra of prolate (top panel) and oblate (bottom panel) silver NPs of different aspect ratio in water, calculated using the *T*-Matrix method.

a nanoparticle, such as DDA, finite difference time-domain or finite element methods. SIE does not require any bounding box to surround the particle and only the surface is meshed, making it less demanding in computational resources than many other methods. Orientation averaging can also be carried out without a significant increase in computing time. We have considered many different types of faceted NPs and show in Fig. 4 the absorption spectra predicted for representative cases: dodecahedra (20 faces), truncated icosahedra (32 faces) and Reuleaux dodecahedra (12 curved faces) of different sizes. Note that all SIE calculated spectra presented here are averaged over 200 NP orientations to be more representative of the experimental conditions (we recall that the sample is a colloidal suspension of NPs in water). While this selection of shapes is unlikely to be representative of actual NP geometries – which result from complex growth mechanisms, and where facets reflect the underlying

1
2
3 crystalline structure of the material – the simulation results suggest general conclusions that
4 do not depend on the particular arrangement of facets, only the departure from sphericity.

5
6
7 We observe that faceting introduces new resonances in the optical response of the NPs,
8 which appear in the sphere's quadrupole resonance region. Remarkably, the NP size only
9 affects the position of the main dipolar resonance (longest wavelength), not that of the
10 extra resonances. Nevertheless, shape does affect the exact position of these resonances,
11 and as illustrated in Fig. 4(d), a distribution of differently-faceted shapes could contribute
12 to washing out the prominent quadrupolar peak predicted for perfect spheres. This would
13 require relatively strong faceting (for example for a dodecahedron), but is not incompatible
14 with the uneven shapes observed in TEM images (inset of Fig. 4(d)). We, therefore, conclude
15 that some degree of random faceting could explain at least to some extent the broad and
16 almost featureless experimental absorption spectrum.
17
18
19
20
21
22
23
24
25
26
27
28

29 **Surface roughness**

30
31 A final source of non-sphericity that we will discuss here is surface roughness. As for the case
32 of NP faceting, many studies on the effect of NP surface roughness on plasmon resonance
33 have been published,^{65–67} with different and sometimes contradicting conclusions.^{31,68} We
34 do not intend here to give a definitive conclusion on the effect of surface roughness on the
35 optical properties of NPs, as it may depend on a number of factors like the NP shape, size,
36 material, detailed type of roughness, etc. Most studies however rely on the comparison
37 between calculations and experimental extinction or scattering spectra alone. Having access
38 to all the far-field optical properties of the NPs provides additional insight, and sharpens
39 the conclusions drawn from the comparison with calculations.
40
41
42
43
44
45
46
47
48

49 We considered roughened spheres with random uncorrelated perturbations of the surface
50 mesh and modeled their optical properties using SIE. The degree of roughness can be char-
51 acterized by the root mean square (rms) average of the local radius deviation (measured
52 from the center of the sphere), denoted δr . We present in Fig. 5 calculations for spheres of
53
54
55
56
57
58
59
60

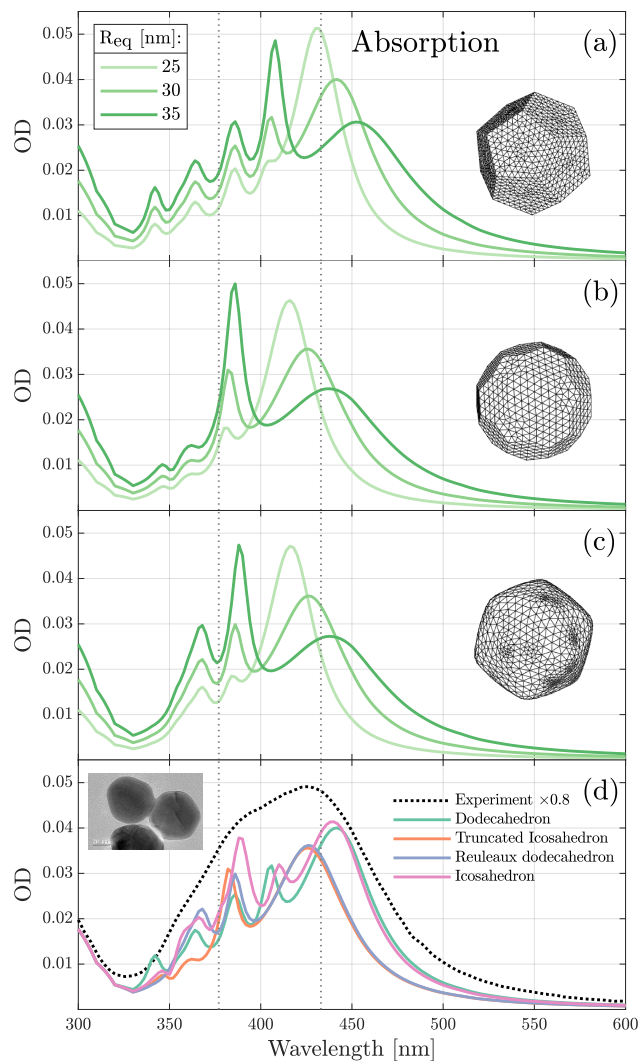


Figure 4: Absorption spectra of three different silver NPs in water calculated by SIE: a dodecahedron (a), a truncated icosahedron (b) and a Reuleaux dodecahedron (c). The three spectra on each panel correspond to different particle size, as characterized by the radius of the equivalent-volume sphere (R_{eq} from 25 to 35 nm). In the bottom panel (d), we superimpose the absorption spectra of different shaped-particle of the same volume ($R_{\text{eq}} = 30$ nm) together with the scaled experimental spectrum. The inset shows a TEM image provided by the manufacturer (Nanocomposix) of the 30 nm radius Ag nanospheres used for the experiment.

average radius 30 nm and rms roughness δr ranging from 0 (sphere) to 1.4 nm. Roughness induces a red-shift in the plasmon resonance positions, both dipolar and quadrupolar, which is observed in extinction, scattering, and absorption. For the highest roughness considered in this simulation (1.4 nm rms, still within a realistic range), the quadrupolar resonance has

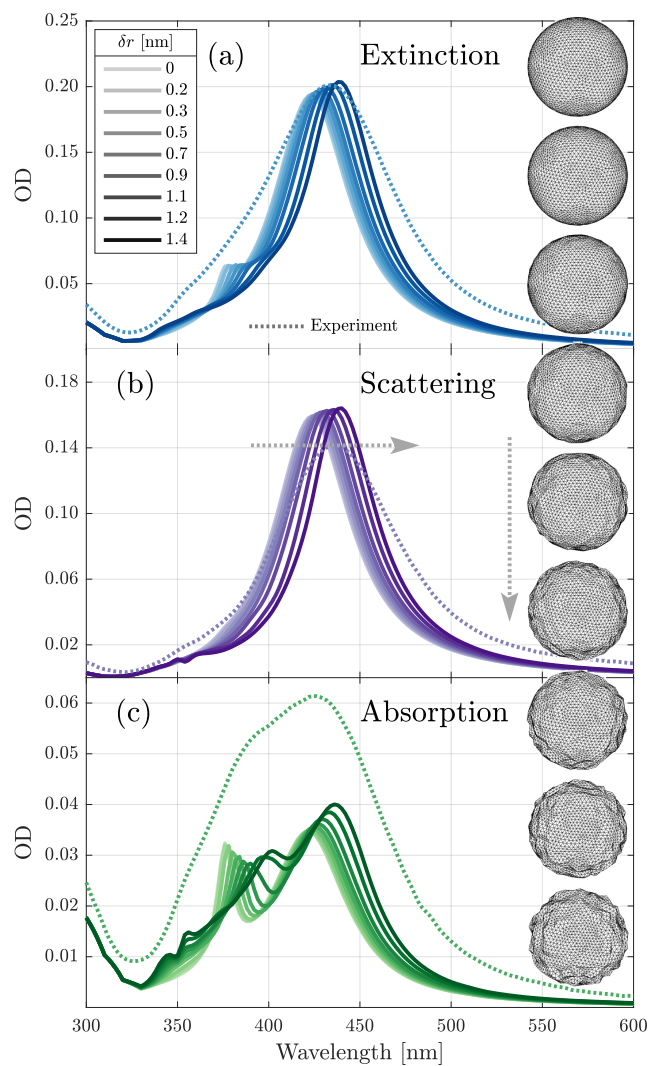


Figure 5: Predicted (from SIE) extinction, scattering and absorption spectra of spherical silver NPs of different rms roughness δr . The NPs are in water and have the same volume as a 60 nm sphere. In each panel, the experimental spectrum is plotted in dotted lines.

broadened to the point where it is no longer prominent in the absorption spectrum and appears as a small shoulder peak. It has also shifted substantially to lie in the middle of the dipole and quadrupole resonance of the perfect sphere. Because this shift strongly depends on the degree of roughness, a distribution of rms roughness could easily broaden and wash out the quadrupole peak to the point where it is no longer visible in absorption. This would also have a limited, hardly-detectable impact on the extinction spectrum, as can be inferred from Fig. 5. These predictions suggest that surface roughness may also play a role in ex-

1
2
3 plaining the experimental absorption spectrum, in addition to the more-easily identifiable
4 faceting discussed earlier. By inspection of Figs. 4 and 5, it appears that disentangling these
5
6
7 two effects will be difficult purely from far-field measurements. Nevertheless, the spectra in
8
9
10 Fig. 4 and 5 demonstrate how sensitive the entire absorption spectrum is to small changes
11
12 on the particle surface (faceting and roughness), in contrast to the extinction and scattering
13
14 spectra, which barely change except for the dipolar resonance. It is also worth pointing out
15
16 that, although outside our scope here, it would be interesting to further test the predictions
17
18 of Fig. 5 experimentally using nanoparticles of varying roughness, for example using chemical
19
20 etching.
21
22

23 **Absolute absorption intensity**

24
25
26 We now come back to our second main observation: the measured absorption spectrum
27
28 appears much more intense than predicted. In fact, we can see from the results of Figs. 3
29
30 to 5 that shape imperfections may affect the spectral profile, but not much the overall
31
32 absorption intensity. Although the NP concentration can be used to scale the predicted
33
34 spectra, it will scale both extinction and absorption, so it cannot explain this discrepancy.
35
36 In order to take the NP concentration out of the equation, it is convenient here to consider
37
38 the ratio η of extinction to absorption. We plot the experimental ratio η in Fig. 6, alongside
39
40 a selection of theoretical predictions. The main discrepancy between experiment and theory
41
42 is observed in the region above 420 nm, i.e. at the dipolar resonance and beyond. The ratio
43
44 η is approximately constant in this region, around 4 in the experiments, but stays around
45
46 6 for predictions with 60 nm NP spheres, even faceted or roughened (keeping the volume-
47
48 equivalent diameter at 60 nm). In all our calculations, we found that the most important
49
50 factor for the extinction to absorption ratio in this region is the particle size, as quantified
51
52 using the NP volume V or the volume-equivalent diameter. This is an important observation
53
54 as this ratio then provides a sensitive measure of nanoparticle volume independent of shape.
55
56 This can be explained in the dipolar approximation, where absorption is proportional to V ,
57
58
59
60

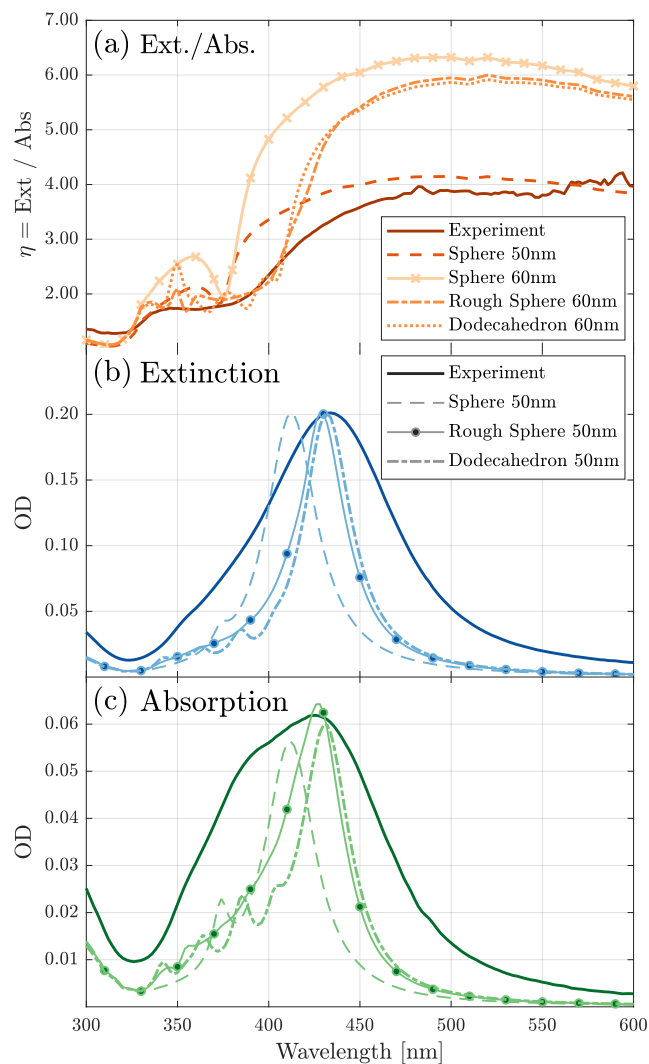


Figure 6: Top panel: ratio of extinction to absorption spectra for our measured NPs (solid line) along with a number of representative predictions: 50 and 60 nm spheres, a 60 nm roughened sphere ($\delta r = 1.4$ nm) and a dodecahedron (radius of the equivalent-volume sphere: 60 nm). Middle and bottom panels: Extinction and absorption spectra for a 50 nm sphere, a rough sphere ($\delta r = 1.4$ nm) and a dodecahedron compared to experiments (solid lines).

1
2
3 while scattering is proportional to V^2 : One therefore expects $\eta - 1$ to be proportional to V .
4

5 We can push predictions for η down to ~ 4 simply by decreasing the particle size down
6 to 50 nm, independent of shape imperfections. This results in a concomitant blue-shift of
7 the plasmon resonance, which for perfect spheres no longer matches the predictions (Fig. 6).
8 However, as discussed earlier, roughness and faceting are accompanied by a red-shift of the
9 resonance, which can in fact compensate the size-induced blue-shift. This is shown in Fig. 6:
10 smaller 50 nm NPs with sufficient roughness or faceting have similar dipolar resonance to a
11 60 nm perfect sphere and can therefore not only match the observed resonances, but also the
12 absolute intensities of both extinction and absorption spectra. Such sizes are still compatible
13 with size estimates from TEM images, because a 50 nm volume-equivalent diameter corre-
14 sponds to larger cord dimensions: The largest cord (“diameter”) of a 50 nm dodecahedron
15 for example is of the order of 56 nm. Failure to account for these shape effects, which are not
16 observable in extinction, results in a large overestimation of the particle volume: a 60-nm
17 volume-equivalent radius instead of 50 nm correspond to a 70% error. More importantly,
18 a similarly large error would result in any estimate of the derived particle concentration
19 from the intensity of the extinction spectrum. Such a large error would have important
20 implications in most contexts.
21
22
23
24
25
26
27
28
29
30
31
32
33
34
35
36

37 It is also worth pointing out here that the extinction to absorption ratio will also be
38 particularly relevant to any type of nanoparticles, not just silver or even metallic ones, as it
39 is always highly sensitive to size except for the smallest sizes (typically smaller than 10 nm
40 diameter). This is illustrated in Fig. 7 for the important case of gold nanoparticles. Inferring
41 the size from the extinction spectrum can be difficult, as the spectrum (once normalized in
42 intensity) barely changes with diameter, especially between 10 and 30 nm (Fig. 7(a)). The
43 absorption spectral shape also hardly changes (not shown), but the ratio $\eta(\lambda)$ does vary
44 significantly (Fig. 7(b)), and therefore provides a robust experimental tool to determine gold
45 NP size.
46
47
48
49
50
51
52
53
54

55 Finally, it is also worth highlighting that a large size distribution will have a different effect
56
57
58
59
60

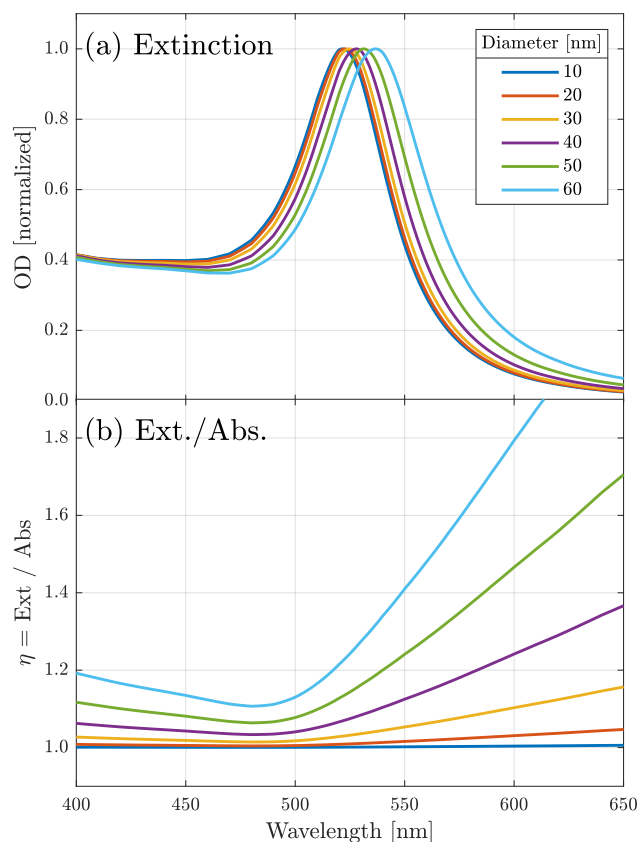


Figure 7: Predicted extinction spectra (a) and extinction to absorption ratios (b) for gold nanospheres of varying diameter in water, calculated using Mie theory and the gold dielectric function from Ref.⁶⁰

on absorption than on extinction. The latter is proportional to V^2 through the scattering contribution, and will therefore be more dominated by larger NP (relative to absorption). The extinction spectrum would then be redshifted compared to the absorption spectrum, although this is likely observable only for relatively large size distribution.

Non-spherical nanoparticles

To show that the results and discussion presented so far are more general than for just spherical nanoparticles, we conclude by considering non-spherical nanoparticles. We focus in particular on 100 nm silver nanocubes.⁶⁹ Their orientation-averaged optical properties can again be predicted using SIE and compared to experiments as summarized in Fig. 8. As

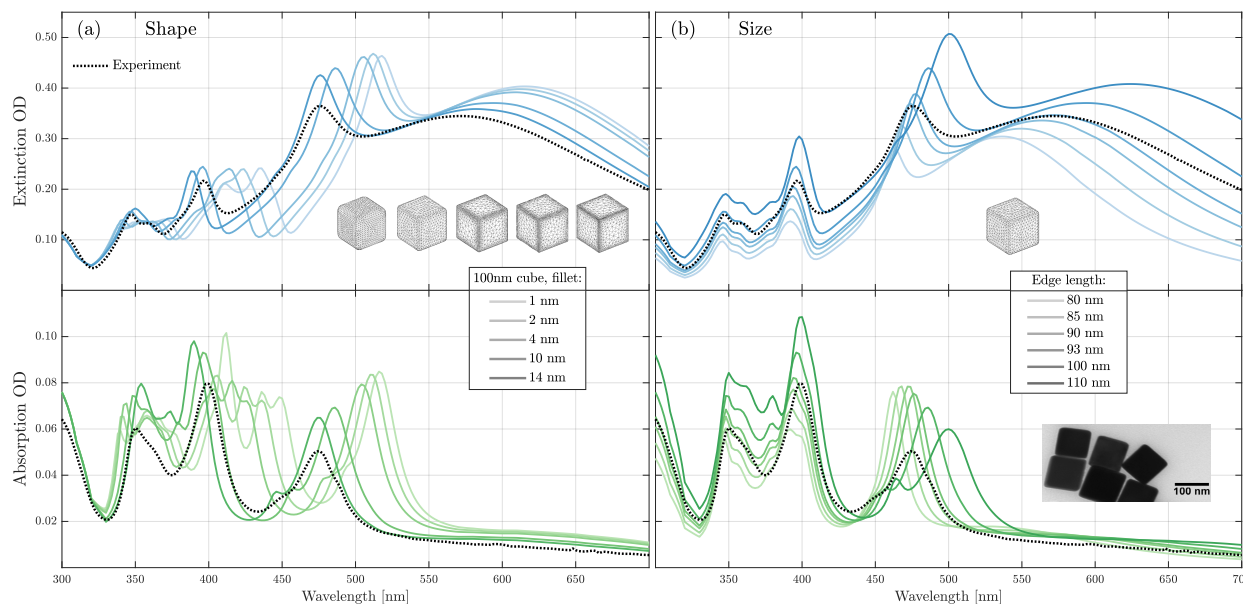


Figure 8: Panel (A): SIE calculated extinction (top) and absorption (bottom) spectra of 100 nm nanocubes with different size of fillet applied to all edges. Panel (B): same as Panel (A) but the cube fillet is fixed at 10 nm and the volume of the cube is varied. In all the panels, the experimental spectra are plotted in dashed lines.

previously reported,^{24,26,29} the extinction spectrum is a lot richer than for spheres, with a broad dipolar resonance at ~ 570 nm and at least three additional higher energy peaks corresponding to higher order resonances. As for spheres, the higher-order resonances are much more prominent in the absorption spectrum, which facilitates their study and comparison with theory. We also note that the dipolar resonance is almost absent from the absorption spectrum, therefore a combined extinction-absorption study is needed to maximize our experimental input. The predicted spectra for a 100 nm nanocube exhibit similar resonances in both extinction and absorption but they are all significantly red-shifted compared to experiment. We would have to bring the edge dimension down to 80 nm to correct this, but this is unrealistic given the TEM images (see inset). We instead consider shape imperfections, as for sphere, and in particular the rounding of the edges and corners, which is in fact apparent in the TEM image. This is accounted for by introducing a fillet on each edge as shown in Fig. 8. This rounding results in a blue-shift of all the resonances and with fillets between 10 nm and 14 nm, several resonances can match the experiments, but not quite all. This

1
2
3 can be further tuned by changing the size for a fixed filet of 10 nm as shown in Fig. 8(b).
4
5 A 93 nm edge-length nanocube with 10 nm filet appears to provide the closer match to the
6
7 experiment in resonance position and intensity for both extinction and absorption. A small
8
9 size distribution could explain the observed broader dipolar resonance in extinction. The
10
11 remaining discrepancy is mostly in the absorption intensity of the ~ 475 nm peak, and ad-
12
13 dressing it would require a more accurate model of the particle geometry. This mode is
14
15 associated with strong field enhancements in the corners²⁹ and we expect that predicting
16
17 the its absorption more accurately will require using a different filet size for corners than
18
19 for edges. That the fine details of the particle's morphology can have notable effects in the
20
21 absorption spectrum presents both a challenge – requiring finer shape characterization –
22
23 and an opportunity: very accurate information on the nanometer scale can be obtained by
24
25 far-field optical measurements
26
27
28

29 Conclusion

30
31
32 This work demonstrates the benefits of measuring both extinction and absorption spectra for
33
34 routine characterization of metallic nanoparticles in solution. While the main dipolar reso-
35
36 nance is most visible in extinction, we have showed that the higher order resonances are much
37
38 more prominent in absorption. We moreover highlighted that these higher order resonances
39
40 are particularly sensitive to small imperfections in NP shape, such as faceting and roughness.
41
42 As a result, many theoretical fits that were acceptable for extinction are not compatible with
43
44 the experimental absorption spectrum. Fitting the latter introduces much tighter constrains
45
46 on the NP geometry, notably the inclusion of roughness and/or faceting. The ratio of ex-
47
48 tinction to absorption also provides an additional experimental constrain, which is primarily
49
50 dictated by the overall particle size, not its shape. We have applied these considerations to
51
52 the canonical system of 60 nm-diameter silver nanospheres and showed that the experimental
53
54 absorption could only be explained by invoking roughness and faceting. This in turn explains
55
56
57
58
59
60

1
2
3 the long-standing puzzle that the quadrupolar resonance is barely observed in the extinc-
4 tion spectrum despite its large prominence in theoretical predictions. It also suggests that
5 large errors in estimated NP volume and concentration may arise when inferring them from
6 the extinction spectrum only. Similar considerations were then applied to silver nanocubes,
7 where the importance of rounding the edges was highlighted. Interestingly, in both cases,
8 the spectra and the ratio of extinction to absorption can all be explained using reported
9 bulk dielectric function for silver, which suggest that there is no need to modify it to account
10 for additional losses due to polycrystallinity or other defects in nanoparticles. We believe
11 this approach is generally applicable to many types of nanoparticles. For the smallest sizes
12 (typically less than 20 nm), scattering is negligible and the absorption spectrum will not
13 add extra insight. But for anything larger, the combination of extinction–absorption spectra
14 provide a much richer, yet simple and easily accessible, characterization of the NP proper-
15 ties. Even for large NPs like the 100 nm nanocubes where scattering dominates, the weaker
16 absorption spectrum still provides more detailed information than the extinction spectrum.
17 These benefits could moreover extend to the characterization of capping molecules adsorbed
18 on the surface of the NPs, which, like roughness, should affect absorption much more than
19 extinction. We believe this approach can be applied to many related systems including
20 dye-coated metallic nanoparticles, for the study of weak and strong plasmon-molecule reso-
21 nance coupling, and other types of non-metallic nanoparticles and microparticles where both
22 absorption and scattering are typically present.
23
24
25
26
27
28
29
30
31
32
33
34
35
36
37
38
39
40
41
42
43
44

45 Methods

46
47
48 **Nanoparticles.** 60 nm citrate-stabilized silver nanoparticles were obtained from Nanocom-
49 posix (USA). The size distribution is provided by the manufacturer. The stock NP colloidal
50 suspension was diluted by a factor of 10 for the measurements. 100 nm Polyvinylpyrroli-
51 done (PVP) coated silver nanocubes (NanoXact) were also obtained from Nanocomposix
52
53
54
55
56
57
58
59
60

1
2
3 (USA). 100 nm-diameter carboxyl-coated amorphous silica sphere were obtained from Mi-
4 cromod (Germany).
5
6
7

8
9 **Absorption/Extinction measurements.** We recorded the optical properties of the
10 Ag NP solution using the CloudSpec-UV-v0.8 from Marama Labs (New Zealand). This in-
11 strument uses an integrating sphere to measure both extinction and absorption spectra of
12 samples. Both are given in units of $[\text{cm}^{-1}]$, i.e. in optical density normalized to a path length
13 of 1 cm. The scattering spectrum can, therefore, be deduced from the difference of both. To
14 check the validity of these spectra, we performed a series of measurements of the Eosin B dye
15 as a function of concentration in water (non-scattering samples). These tests (see Fig. S1)
16 confirmed that the extinction and absorption spectra were the same and were linear over the
17 concentration range of interest. Similar measurements were then carried out in the presence
18 of scattering by adding 300 nm-diameter carboxyl-coated silica spheres (whose concentration
19 was adjusted to match the Ag NP scattering at resonance). The absorption spectra were
20 the same as those measured in the absence of scattering in water, as expected, see Fig. S1
21 in Suppl. info. Finally, measurements on the NPs were performed for three dilution factors,
22 namely 5, 10 and 40, and gave the same spectrum when adjusted by the corresponding factor
23 (see Fig. S2).
24
25
26
27
28
29
30
31
32
33
34
35
36
37
38
39
40

41 **Mie theory.** Mie theory calculations were performed using the SPlac package.^{56,70} In all
42 EM calculations, the wavelength-dependent refractive index for water was taken from Ref.⁷¹
43 Except where specified in the main text, the dielectric function for silver were taken from
44 Ref.⁵⁷ (Sample C, `AgC_corrected.csv`, as provided in the supporting information of⁵⁷).
45
46
47
48
49
50

51 **Calculations on elongated NPs.** The optical properties of spheroidal NPs were computed
52 using SMARTIES,⁷² which provides a Matlab implementation of the *T*-Matrix method with
53 recently developed improved algorithms specially developed for spheroidal nanoparticles.^{73,74}
54
55
56
57
58
59
60

1
2
3 An estimate of the accuracy of the results is returned by the computation and high accuracy
4 (comparable to Mie theory, better than 10^{-12})¹⁷ is achieved for all the examples considered
5 here.
6
7
8
9

10
11 **Surface integral equation calculations.** For other non-spherical particles, the surface-
12 integral equation formalism was used.^{18,64} We have used an implementation specially devel-
13 oped (and tested) for plasmonics and metallic nanoparticles.¹⁹ The quality of the mesh in
14 each case is illustrated in the corresponding figures. To create the roughened sphere, we
15 started from a coarse mesh of 630 nodes and for each node, the distance from the origin was
16 multiplied by a factor $1 + \kappa u$, where u is a random number between -1 and 1 . The degree of
17 roughness can be adjusted by changing κ . The resulting mesh was then further refined (2514
18 nodes) to improve the accuracy of the calculation. We checked that the predicted spectra
19 were almost identical for two different roughened sphere generated with the same κ .
20
21
22
23
24
25
26
27
28
29
30

31 Acknowledgement

32
33
34 The authors thank the Royal Society Te Apārangi for support through a Rutherford Discov-
35 ery Fellowship (B.A.) and a Marsden grant (J.G. and E.C.L.R.). We are grateful to Marama
36 Labs Ltd for providing us early access to their prototype instrument. We are grateful to
37 Nanocomposix for providing us with silver nanocubes.
38
39
40
41
42
43
44

45 Supporting Information Available

46
47
48 Supplementary information is available.

49
50 pdf file: Additional figures S1 and S2 confirming the validity of the scattering-independent
51 absorption spectra.
52
53
54
55
56
57
58
59
60

Conflict of Interest

The instrument used for the measurements discussed in this manuscript was developed and is commercialized by Marama Labs, a start-up company that was spun out from our research. As a consequence, two of the authors (BA and ECLR) have a small share in this company.

References

- (1) Patra, J. K.; Das, G.; Fraceto, L. F.; Campos, E. V. R.; Rodriguez-Torres, M. d. P.; Acosta-Torres, L. S.; Diaz-Torres, L. A.; Grillo, R.; Swamy, M. K.; Sharma, S.; Habtemariam, S.; Shin, H.-S. Nano based drug delivery systems: recent developments and future prospects. *Journal of Nanobiotechnology* **2018**, *16*, 71.
- (2) Rodrigues, T. S.; da Silva, A. G. M.; Camargo, P. H. C. Nanocatalysis by noble metal nanoparticles: controlled synthesis for the optimization and understanding of activities. *J. Mater. Chem. A* **2019**, *7*, 5857–5874.
- (3) Le Ru, E. C.; Etchegoin, P. G. Single molecule analysis by surfaced-enhanced Raman scattering. *Annu. Rev. Phys. Chem.* **2012**, *63*, 65.
- (4) Mubeen, S.; Lee, J.; Lee, W.-r.; Singh, N.; Stucky, G. D.; Moskovits, M. On the Plasmonic Photovoltaic. *ACS Nano* **2014**, *8*, 6066–6073.
- (5) Haiss, W.; Thanh, N. T. K.; Aveyard, J.; Fernig, D. G. Determination of Size and Concentration of Gold Nanoparticles from UV-Vis Spectra. *Anal. Chem.* **2007**, *79*, 4215–4221.
- (6) Mie, G. Contributions to the optics of turbid media, particularly of colloidal metal solutions. *Ann. Phys.* **1908**, *25*, 377–445.
- (7) Bohren, C. F.; Huffman, D. R. *Absorption and scattering of light by small particles*; John Wiley & Sons Inc.: New York, 1983.

- 1
2
3 (8) Hao, F.; Nordlander, P. Efficient dielectric function for FDTD simulation of the optical
4 properties of silver and gold nanoparticles. *Chem. Phys. Lett.* **2007**, *446*, 115 – 118.
5
6
7
8 (9) Khoury, C. G.; Norton, S. J.; Vo-Dinh, T. Plasmonics of 3-D Nanoshell Dimers Using
9 Multipole Expansion and Finite Element Method. *ACS Nano* **2009**, *3*, 2776–2788.
10
11
12 (10) Yang, W.-H.; Schatz, G. C.; Duynes, R. P. V. Discrete dipole approximation for cal-
13 culating extinction and Raman intensities for small particles with arbitrary shapes. *J.*
14 *Chem. Phys.* **1995**, *103*, 869–875.
15
16
17
18 (11) Yurkin, M.; Hoekstra, A. The discrete-dipole-approximation code ADDA: capabilities
19 and known limitations. *J. Quant. Spectrosc. Rad. Transfer* **2011**, *112*, 2234–2247.
20
21
22 (12) Hoffmann, J.; Hafner, C.; Leidenberger, P.; Hesselbartha, J.; Burgerb, S. Comparison
23 of electromagnetic field solvers for the 3D analysis of plasmonic nano antennas. *Proc.*
24 *SPIE* **2009**, *7390*.
25
26
27
28 (13) Lesina, A. C.; Vaccari, A.; Berini, P.; Ramunno, L. On the convergence and accuracy
29 of the FDTD method for nanoplasmonics. *Opt. Express* **2015**, *23*, 10481–10497.
30
31
32 (14) Kupresak, M.; Zheng, X.; Vandenbosch, G. A. E.; Moshchalkov, V. V. Benchmarking of
33 software tools for the characterization of nanoparticles. *Opt. Express* **2017**, *25*, 26760–
34 26780.
35
36
37 (15) Waterman, P. C. Matrix formulation of electromagnetic scattering. *Proc. IEEE* **1965**,
38 *53*, 805–812.
39
40
41 (16) Mishchenko, M. I.; Travis, L. D.; Lacis, A. A. *Scattering, absorption and emission of*
42 *light by small particles*, 3rd ed.; Cambridge University Press: Cambridge, 2002.
43
44
45
46 (17) Somerville, W. R. C.; Auguié, B.; Le Ru, E. C. Accurate and convergent T-matrix
47 calculations of light scattering by spheroids. *J. Quant. Spectrosc. Rad. Transfer* **2015**,
48 *160*, 29–35.
49
50
51
52
53
54
55
56
57
58
59
60

- 1
2
3 (18) Kern, A. M.; Martin, O. J. F. Surface integral formulation for 3D simulations of plas-
4 monic and high permittivity nanostructures. *J. Opt. Soc. Am. A* **2009**, *26*, 732–740.
5
6
7
8 (19) Raziman, T. V.; Somerville, W. R. C.; Martin, O. J. F.; Le Ru, E. C. Accuracy of
9 Surface Integral Equation Matrix Elements in Plasmonic Calculations. *Journal of the*
10 *Optical Society of America B* **2015**, *32*, 485.
11
12
13
14 (20) Schebarchov, D.; Auguie, B.; Le Ru, E. C. Simple accurate approximations for the
15 optical properties of metallic nanospheres and nanoshells. *Phys. Chem. Chem. Phys.*
16 **2013**, *15*, 4233–4242.
17
18
19
20
21 (21) Majic, M. R. A.; Pratley, L.; Schebarchov, D.; Somerville, W. R. C.; Auguie, B.; Le
22 Ru, E. C. Approximate T matrix and optical properties of spheroidal particles to third
23 order with respect to size parameter. *Phys. Rev. A* **2019**, *99*, 013853.
24
25
26
27
28 (22) Yu, R.; Liz-Marzán, L. M.; García de Abajo, F. J. Universal analytical modeling of
29 plasmonic nanoparticles. *Chem. Soc. Rev.* **2017**, *46*, 6710–6724.
30
31
32
33 (23) Russell, B. K.; Mantovani, J. G.; Anderson, V. E.; Warmack, R. J.; Ferrell, T. L.
34 Experimental Test of the Mie Theory for Microlithographically Produced Silver Spheres.
35 *prb* **1987**, *35*, 2151–2154.
36
37
38
39 (24) Sherry, L. J.; Chang, S.-H.; Schatz, G. C.; Van Duyne, R. P.; Wiley, B. J.; Xia, Y.
40 Localized Surface Plasmon Resonance Spectroscopy of Single Silver Nanocubes. *Nano*
41 *Lett.* **2005**, *5*, 2034–2038.
42
43
44
45 (25) Tao, A.; Sinsermsuksakul, P.; Yang, P. Polyhedral Silver Nanocrystals with Distinct
46 Scattering Signatures. *Angew. Chem. Internat. Ed.* **2006**, *45*, 4597–4601.
47
48
49
50 (26) McMahon, J. M.; Wang, Y.; Sherry, L. J.; Van Duyne, R. P.; Marks, L. D.; Gray, S. K.;
51 Schatz, G. C. Correlating the Structure, Optical Spectra, and Electrodynamics of Single
52 Silver Nanocubes. *J. Phys. Chem. C* **2009**, *113*, 2731–2735.
53
54
55
56
57
58
59
60

- 1
2
3
4 (27) Rodríguez-Fernández, J.; Novo, C.; Myroshnychenko, V.; Funston, A. M.; Sánchez-
5 Iglesias, A.; Pastoriza-Santos, I.; Pérez-Juste, J.; García de Abajo, F. J.; Liz-
6 Marzán, L. M.; Mulvaney, P. Spectroscopy, Imaging, and Modeling of Individual Gold
7 Decahedra. *J. Phys. Chem. C* **2009**, *113*, 18623–18631.
8
9
10
11
12 (28) Henry, A.-I.; Bingham, J. M.; Ringe, E.; Marks, L. D.; Schatz, G. C.; Van Duyne, R. P.
13 Correlated Structure and Optical Property Studies of Plasmonic Nanoparticles. *J. Phys.*
14 *Chem. C* **2011**, *115*, 9291–9305.
15
16
17
18 (29) Mahmoud, M. A.; Chamanzar, M.; Adibi, A.; El-Sayed, M. A. Effect of the Dielec-
19 tric Constant of the Surrounding Medium and the Substrate on the Surface Plas-
20 mon Resonance Spectrum and Sensitivity Factors of Highly Symmetric Systems: Silver
21 Nanocubes. *J. Am. Chem. Soc.* **2012**, *134*, 6434–6442.
22
23
24
25
26
27 (30) Wang, H.; Fu, K.; Drezek, R.; Halas, N. Light scattering from spherical plasmonic
28 nanoantennas: effects of nanoscale roughness. *Appl. Phys. B* **2006**, *84*, 191–195.
29
30
31
32 (31) Trügler, A.; Tinguely, J.-C.; Krenn, J. R.; Hohenau, U., A. and Hohenester Influence of
33 surface roughness on the optical properties of plasmonic nanoparticles. *Phys. Rev. B*
34 **2011**, *83*, 081412.
35
36
37
38 (32) Jiang, Y.; Pillai, S.; Green, M. A. Realistic Silver Optical Constants for Plasmonics.
39 *Phys. Rev. B* **2012**, *86*, 235147.
40
41
42
43 (33) Huang, X.; El-Sayed, I. H.; Qian, W.; El-Sayed, M. A. Cancer Cell Imaging and Pho-
44 tothermal Therapy in the Near-Infrared Region by Using Gold Nanorods. *J. Am. Chem.*
45 *Soc.* **2006**, *128*, 2115–2120.
46
47
48
49 (34) McFarland, A. D.; Van Duyne, R. P. Single Silver Nanoparticles as Real-Time Optical
50 Sensors with Zeptomole Sensitivity. *Nano Lett.* **2003**, *3*, 1057–1062.
51
52
53
54
55
56
57
58
59
60

- 1
2
3 (35) Kreibig, U.; Schmitz, B.; Breuer, H. D. Separation of plasmon-polariton modes of small
4 metal particles. *Phys. Rev. B* **1987**, *36*, 5027–5030.
5
6
7
8 (36) Arbouet, A.; Christofilos, D.; Del Fatti, N.; Vallée, F.; Huntzinger, J. R.; Arnaud, L.;
9 Billaud, P.; Broyer, M. Direct Measurement of the Single-Metal-Cluster Optical Ab-
10 sorption. *Phys. Rev. Lett.* **2004**, *93*, 127401.
11
12
13
14 (37) Tcherniak, A.; Ha, J. W.; Dominguez-Medina, S.; Slaughter, L. S.; Link, S. Probing
15 a Century Old Prediction One Plasmonic Particle at a Time. *Nano Lett.* **2010**, *10*,
16 1398–1404.
17
18
19
20
21 (38) Husnik, M.; Linden, S.; Diehl, R.; Niegemann, J.; Busch, K.; Wegener, M. Quantitative
22 Experimental Determination of Scattering and Absorption Cross-Section Spectra of
23 Individual Optical Metallic Nanoantennas. *Phys. Rev. Lett.* **2012**, *109*, 233902.
24
25
26
27
28 (39) Micali, N.; Mallamace, F.; Castriciano, M.; Romeo, A.; Monsú Scolaro, L. Separation of
29 Scattering and Absorption Contributions in UV/Visible Spectra of Resonant Systems.
30 *Anal. Chem.* **2001**, *73*, 4958–4963.
31
32
33
34
35 (40) Liu, B.-J.; Lin, K.-Q.; Hu, S.; Wang, X.; Lei, Z.-C.; Lin, H.-X.; Ren, B. Extraction
36 of Absorption and Scattering Contribution of Metallic Nanoparticles Toward Rational
37 Synthesis and Application. *Anal. Chem.* **2015**, *87*, 1058–1065.
38
39
40
41
42 (41) Nelson, N. B.; Prézelin, B. B. Calibration of an integrating sphere for determining the
43 absorption coefficient of scattering suspensions. *Appl. Opt.* **1993**, *32*, 6710–6717.
44
45
46
47 (42) Babin, M.; Stramski, D. Light absorption by aquatic particles in the near-IR spectral
48 region. *Limnol. Oceanogr.* **2002**, *47*, 911–915.
49
50
51
52 (43) Tassan, S.; Ferrari, G. M. Variability of light absorption by aquatic particles in the
53 near-IR spectral region. *Appl. Opt.* **2003**, *42*, 4802–4810.
54
55
56
57
58
59
60

- 1
2
3 (44) Gaigalas, A. K.; He, H.-J.; Wang, L. Measurement of absorption and scattering with
4 an integrating sphere detector: application to microalgae. *J. Res. Natl. Inst. Stand.*
5 *Technol.* **2009**, *114*, 69–81.
6
7
8
9
10 (45) Evanoff, D. D.; Chumanov, G. Size-Controlled Synthesis of Nanoparticles. 2. Measure-
11 ment of Extinction, Scattering, and Absorption Cross Sections. *J. Phys. Chem. B* **2004**,
12 *108*, 13957–13962.
13
14
15
16 (46) Darby, B. L.; Auguie, B.; Meyer, M.; Pantoja, A. E.; Le Ru, E. C. Modified opti-
17 cal absorption of molecules on metallic nanoparticles at sub-monolayer coverage. *Nat.*
18 *Photon.* **2016**, *10*, 40–45.
19
20
21
22
23 (47) Villanueva, Y.; Veenstra, C.; Steenbergen, W. Measuring absorption coefficient of scat-
24 tering liquids using a tube inside an integrating sphere. *Appl. Opt.* **2016**, *55*, 3030–3038.
25
26
27
28 (48) Tang, C.; Meyer, M.; Darby, B. L.; Auguie, B.; Le Ru, E. C. Realistic ports in inte-
29 grating spheres: reflectance, transmittance, and angular redirection. *Appl. Opt.* **2018**,
30 *57*, 1581–1588.
31
32
33
34
35 (49) Le Ru, E. C.; Blackie, E.; Meyer, M.; Etchegoin, P. G. SERS enhancement factors: a
36 comprehensive study. *J. Phys. Chem. C* **2007**, *111*, 13794–13803.
37
38
39
40 (50) Le Ru, E. C.; Meyer, M.; Etchegoin, P. G. Proof of single-molecule sensitivity in surface
41 enhanced Raman scattering (SERS) by means of a two-analyte technique. *J. Phys.*
42 *Chem. B* **2006**, *110*, 1944–1948.
43
44
45
46 (51) Blackie, E. J.; Le Ru, E. C.; Etchegoin, P. G. Single molecule surface-enhanced Raman
47 spectroscopy of non-resonant molecules. *J. Am. Chem. Soc.* **2009**, *131*, 14466–14472.
48
49
50
51 (52) Etchegoin, P. G.; Le Ru, E. C.; Meyer, M. Evidence of Natural Isotopic Distribution
52 from Single-Molecule SERS. *J. Am. Chem. Soc.* **2009**, *131*, 2713–2716.
53
54
55
56
57
58
59
60

- 1
2
3 (53) Galloway, C. M.; Etchegoin, P. G.; Le Ru, E. C. Ultrafast nonradiative decay rates
4 on metallic surfaces by comparing surface-enhanced Raman and fluorescence signals of
5 single molecules. *Phys. Rev. Lett.* **2009**, *103*, 063003.
6
7
8
9
10 (54) McPeak, K. M.; Jayanti, S. V.; Kress, S. J. P.; Meyer, S.; Iotti, S.; Rossinelli, A.;
11 Norris, D. J. Plasmonic Films Can Easily Be Better: Rules and Recipes. *ACS Photonics*
12 **2015**, *2*, 326–333.
13
14
15
16 (55) David, R.; Simon, V.; Sébastien, B.; Philip, M.; Eric, M.; Michel, M. An Analytic
17 Model for the Dielectric Function of Au, Ag, and their Alloys. *Adv. Opt. Mater.* **2014**,
18 *2*, 176–182.
19
20
21
22 (56) Le Ru, E. C.; Etchegoin, P. G. *Principles of surface-enhanced Raman spectroscopy and*
23 *related plasmonic effects*; Elsevier: Amsterdam, 2009.
24
25
26
27 (57) Yang, H. U.; D'Archangel, J.; Sundheimer, M. L.; Tucker, E.; Boreman, G. D.;
28 Raschke, M. B. Optical dielectric function of silver. *Phys. Rev. B* **2015**, *91*, 235137.
29
30
31
32 (58) Johnson, P. B.; Christy, R. W. Optical Constants of the Noble Metals. *Physical Review*
33 *B* **1972**, *6*, 4370–4379.
34
35
36
37 (59) Etchegoin, P. G.; Le Ru, E. C.; Meyer, M. An analytic model for the optical properties
38 of gold. *J. Chem. Phys.* **2006**, *125*, 164705.
39
40
41
42 (60) Olmon, R. L.; Slovick, B.; Johnson, T. W.; Shelton, D.; Oh, S.-H.; Boreman, G. D.;
43 Raschke, M. B. Optical dielectric function of gold. *Phys. Rev. B* **2012**, *86*, 235147.
44
45
46
47 (61) Jiang, Y.; Pillai, S.; Green, M. A. Re-evaluation of literature values of silver optical
48 constants. *Opt. Express* **2015**, *23*, 2133–2144.
49
50
51
52 (62) Schiebener, P.; Straub, J.; Levelt Sengers, J. M. H.; Gallagher, J. S. Refractive index of
53 water and steam as function of wavelength, temperature and density. *J. Phys. Chem.*
54 *Ref. Data* **1990**, *19*, 677–717.
55
56
57
58
59
60

- 1
2
3 (63) Tao, A. R.; Habas, S.; Yang, P. Shape Control of Colloidal Metal Nanocrystals. *Small*
4 **2008**, *4*, 310–325.
5
6
7
8 (64) Kern, A. M.; Martin, O. J. F. Excitation and Reemission of Molecules near Realistic
9 Plasmonic Nanostructures. *Nano Lett.* **2011**, *11*, 482–487.
10
11
12 (65) Rodríguez-Fernández, J.; Funston, A. M.; Pérez-Juste, J.; Álvarez-Puebla, R. A.; Liz-
13 Marzán, L. M.; Mulvaney, P. The Effect of Surface Roughness on the Plasmonic Re-
14 sponse of Individual Sub-Micron Gold Spheres. *Phys. Chem. Chem. Phys.* **2009**, *11*,
15 5909.
16
17
18
19
20
21 (66) Perassi, E. M.; Hernandez-Garrido, J. C.; Moreno, M. S.; Encina, E. R.; Coron-
22 ado, E. A.; Midgley, P. A. Using Highly Accurate 3D Nanometrology to Model the
23 Optical Properties of Highly Irregular Nanoparticles: A Powerful Tool for Rational
24 Design of Plasmonic Devices. *Nano Lett.* **2010**, *10*, 2097–2104.
25
26
27
28
29
30 (67) Hong, S.; Shuford, K. L.; Park, S. Observation of a Quadrupole Surface Plasmon Mode
31 for Au Nanorods: Effects of Surface Roughness and Crystal Facets. *Chemistry - An*
32 *Asian Journal* **2013**, *8*, 1259–1264.
33
34
35
36
37 (68) Pecharromán, C.; Pérez-Juste, J.; Mata-Osoro, G.; Liz-Marzán, L. M.; Mulvaney, P.
38 Redshift of Surface Plasmon Modes of Small Gold Rods Due to Their Atomic Roughness
39 and End-Cap Geometry. *Phys. Rev. B* **2008**, *77*, 035418.
40
41
42
43
44 (69) Sun, Y.; Xia, Y. Shape-Controlled Synthesis of Gold and Silver Nanoparticles. *Science*
45 **2002**, *298*, 2176–2179.
46
47
48
49 (70) Le Ru, E. C.; Etchegoin, P. G. SERS and Plasmonics Codes (SPlaC). Matlab codes
50 freely available from <http://www.vuw.ac.nz/raman/book/codes.aspx>, 2009.
51
52
53
54 (71) Harvey, A. H.; Gallagher, J. S.; Sengers, J. M. H. L. Revised Formulation for the
55
56
57
58
59
60

1
2
3 Refractive Index of Water and Steam as a Function of Wavelength, Temperature and
4 Density. *J. Phys. Chem. Reference Data* **1998**, *27*, 761–774.
5
6

7
8 (72) Somerville, W. R. C.; Auguié, B.; Le Ru, E. C. SMARTIES: User-friendly codes for
9 fast and accurate calculations of light scattering by spheroids. *J. Quant. Spectrosc. Rad.*
10 *Transfer* **2016**, *174*, 39 – 55.
11
12

13
14
15 (73) Somerville, W. R. C.; Auguié, B.; Le Ru, E. C. Severe loss of precision in calculations
16 of T-matrix integrals. *J. Quant. Spectrosc. Rad. Transfer* **2012**, *113*, 524 – 535.
17
18

19
20 (74) Somerville, W. R. C.; Auguié, B.; Le Ru, E. C. A new numerically stable implementa-
21 tion of the T-matrix method for electromagnetic scattering by spheroidal particles. *J.*
22 *Quant. Spectrosc. Rad. Transfer* **2013**, *123*, 153–168.
23
24
25
26
27
28
29
30
31
32
33
34
35
36
37
38
39
40
41
42
43
44
45
46
47
48
49
50
51
52
53
54
55
56
57
58
59
60

Graphical TOC Entry

